Backflow vortex behaviours in contra-rotating axial flow pump at low flow rates

To cite this article: D Zhang *et al* 2018 *IOP Conf. Ser.: Earth Environ. Sci.* **163** 012036

IOP Conf. Series: Earth and Environmental Science **163** (2018) 012036 doi:10.1088/1755-1315/163/1/012036

Backflow vortex behaviours in contra-rotating axial flow pump at low flow rates

D Zhang[1], T Tsuneda[1], Y Katayama[2], S Watanabe[2], S I Tsuda[2] and A Furukawa[3]

[1]Graduate School of Engineering, Kyushu University, Fukuoka, Japan
[2]Department of Mechanical Engineering, Kyushu University, Fukuoka, Japan
[3]National Institute of Technology, Oita College, Oita, Japan

fmnabe@mech.kyushu-u.ac.jp

Abstract. Backflow usually exists at the inlet of rotors of many turbomachines at low flow rates. In counter-rotating rotors applied for the axial flow pump, such vortical structures are also able to form. In our previous researches, some broad-banded pressure fluctuations in low frequency range have been observed between front and rear rotors, but we have not yet been able to explain what causes such phenomenon. In this study, in order to find out the causes of low frequency components at low flow rates, unsteady numerical simulations for the whole front and rear rotors are conducted, and casing pressure is experimentally measured at the inlet and outlet of front rotor and the inlet of rear rotor. It is found that vortical structures exist between front and rear rotors at below 40% of design flow rate. These vortices seem to be the result of shear layer instability at the impingement location of the exiting flow from front rotor to the backflow of rear rotor. The behaviours of these backflow vortices and their interaction with front rotor contribute the low frequency components in pressure fluctuations observed at low flow rates.

1. Introduction

It is well known that backflow occurs at the inlet of pump/fan/compressor rotors at low flow rates, and the backflow region increases with the decrease of flow rate. Yokota et al [1] have observed vortex structures at the inlet of an inducer in experiment, and these vortices have been confirmed to be caused by the strong circumferential shear flow between the swirling backflow and the oncoming main flow. A numerical research based on Large Eddy Simulation (LES) is conducted by Yamanishi et al [2] to investigate the backflow vortex structure at the inlet of an inducer. Depending on the number of vortices and their moving velocities in circumferential direction, the backflow vortices induce pressure fluctuations with high frequency, which are afraid to cause some structural troubles and mechanical vibrations.

In contra-rotating axial flow pumps, such vortical flow structures may be also able to form. Actually, in our previous study [3] aiming at understanding the pressure fluctuations due to rotor-rotor interactions, some broad-banded pressure fluctuations in low frequency range are observed in the gap between the front and rear rotors. Since the flow is too complex, it is very difficult to understand the flow mechanism causing such pressure fluctuations only through experiment. Therefore, in this study, unsteady numerical simulations considering the whole front and rear rotors are conducted at different low flow rates. Special emphasis is placed on the vortical structures between the front and rear rotors, which may induce the above-mentioned low frequency pressure fluctuations. By conducting experiments below 30% of design flow rates, fluctuating pressure signals are measured at the inlet of front rotor, outlet of front rotor and inlet of rear rotor.

In the present paper, by using numerical results, we will explain that these vortices between front and rear rotors originate from the boundary between main flow and backflow regions. The vortex behaviors will be used to understand the frequency-domain pressure signals measured in experiments.

2. Methods

The test contra-rotating axial flow pump has been designed with different speed of front and rear rotors [4]. By considering higher cavitation performance of rear rotor, as well as the design flow rate Q_d =70 L/s and total design head $H_{d,t}$ =4 m, the optimized rotational speed combination was determined: rotational speed of front rotor N_f =1311 rpm, rotational speed of rear rotor N_r =1123 rpm. The diameter of hub is 100 mm, while the diameter of casing D_c =200 mm, and the blade tip clearance is 1mm. The blade numbers of front and rear rotors are 4 and 5 respectively. For more detail of the design were shown in the reference [4].

2.1. Numerical simulation

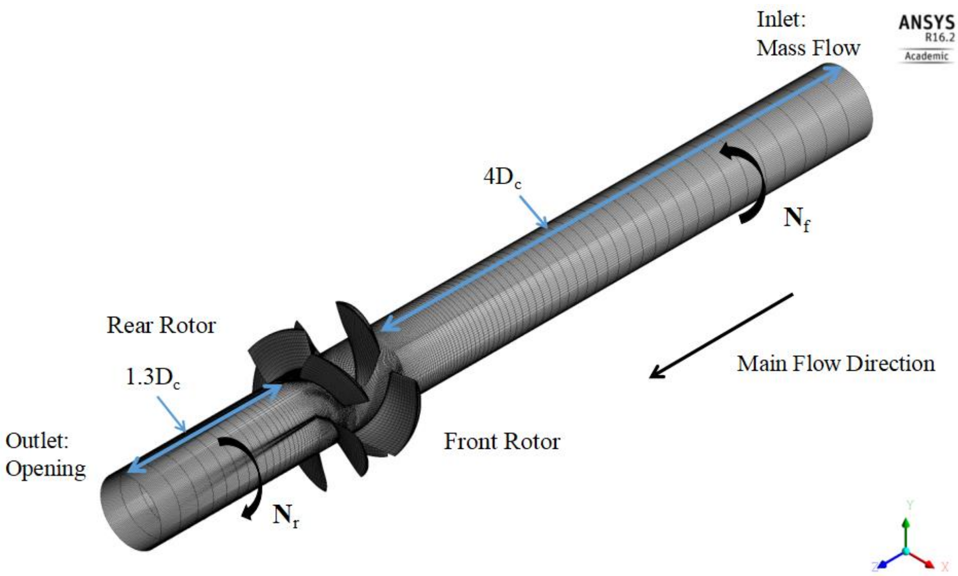

Figure 1. Numerical model

Numerical simulations are conducted by using a commercial CFD code, ANSYS CFX 16.2. As shown in figure 1, the whole front and rear rotors are modelled. The inlet boundary is located at 4D_c upstream of the leading edge of front rotor, while the outlet boundary is located at 1.3D_c downstream of the trailing edge of rear rotor. Furthermore, the inlet boundary type is chosen for the inlet boundary with specifying the mass flow rate, and the opening boundary type is chosen for the outlet boundary with constant static pressure. In the numerical model, two domains have been built up: Front Rotor and Rear Rotor. The total number of nodes in both of domains is over 1.5 million, and at the same time, 10 nodes are radially located in the blade tip clearance to reproduce the tip leakage flow.

Even though the Large Eddy Simulation (LES) should be more appropriate to predict the unsteady flow field. The pump performance and internal flow have been well predicted by using the unsteady Reynolds Averaged Navier Stokes (RANS) based simulation as shown in our previous study. Therefore, the unsteady RANS based simulation is again used in the present study. As will be shown later, the RANS based numerical results can provide us with sufficient information to understand the frequency distribution of pressure fluctuation measured in experiments. Furthermore, the k-ω based SST (Shear Stress Transfer) turbulence model is selected to well predict the flow separation.

The time step in this study is determined with the following equation:

$$\Delta t = \frac{0.5°}{360°} \times \frac{60\ [s/min]}{N_f + N_r} \tag{1}$$

This time step represents the time duration of 0.5 degree relative rotation of front and rear rotors. All the simulations have been conducted over 5 full relative revolutions, where stable flow variable fluctuations are achieved. The quasi-steady results are used to analyse the vortical structures.

2.2. Experimental setup

In order to measure the pressure signals at the inlet of front rotor (Ch.1), outlet of front rotor (Ch.2) and inlet of rear rotor (Ch.3), three pressure transducers have been set in the three positions displayed in figure 2. These pressure taps will collect 2^{20} (1048576) samples with 10kHz sampling frequency.

All the pressures are processed for the Fast-Fourier Transformation (FFT). In order to achieve fine frequency resolution, the whole samples of pressures are divided into 63 parts, and each part has 50% overlap with the adjacent part, then average spectral of every part's FFT results is obtained.

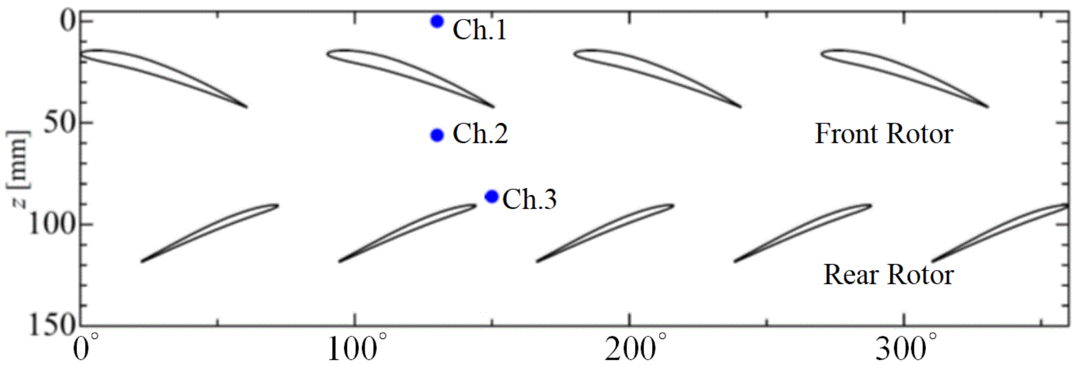

Figure 2. Pressure taps position

3. Results and discussions

3.1. The origin of vortices

As shown in figure 3, vortex structures can be seen in the gap region between front and rear rotors. These vortex structures are observed only at the flow rates below 27 L/s (about 40% of design flow rate). The circumferential velocity normalized by front rotor tip velocity are used to display the main flow and backflow regions in the figure. The positive value represents the flow swirling in front rotor rotating direction, which shows the flow is exiting from the front rotor. On the other hand, the negative value represents the flow swirling in rear rotor rotating direction, which indicates this region is the backflow region from the rear rotor. As we can see, the vortex cores just exist on the boundary of main flow region (red colour) and backflow region of rear rotor (blue colour). This indicates these vortices may be the result of shear layer instability between the main flow and the rear rotor backflow. In order to confirm the origin of these vortex structures, we compare the axial positions of backflow region boundary and vortex cores. At the same time, the observed circumferential moving velocity of vortex cores will be compared with the calculated velocity by using circumferential velocity of main flow and backflow of rear rotor.

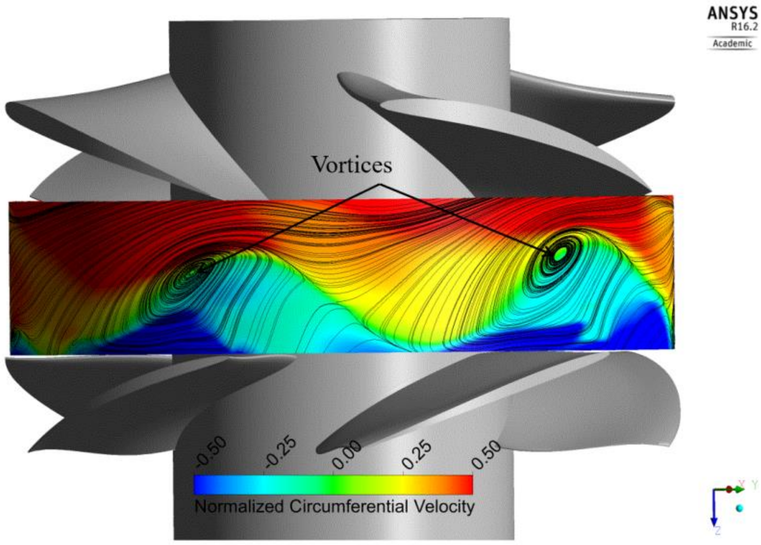

Figure 3. Vortex structures and normalized circumferential velocity distribution on 0.975 span at 30% of design flow rate

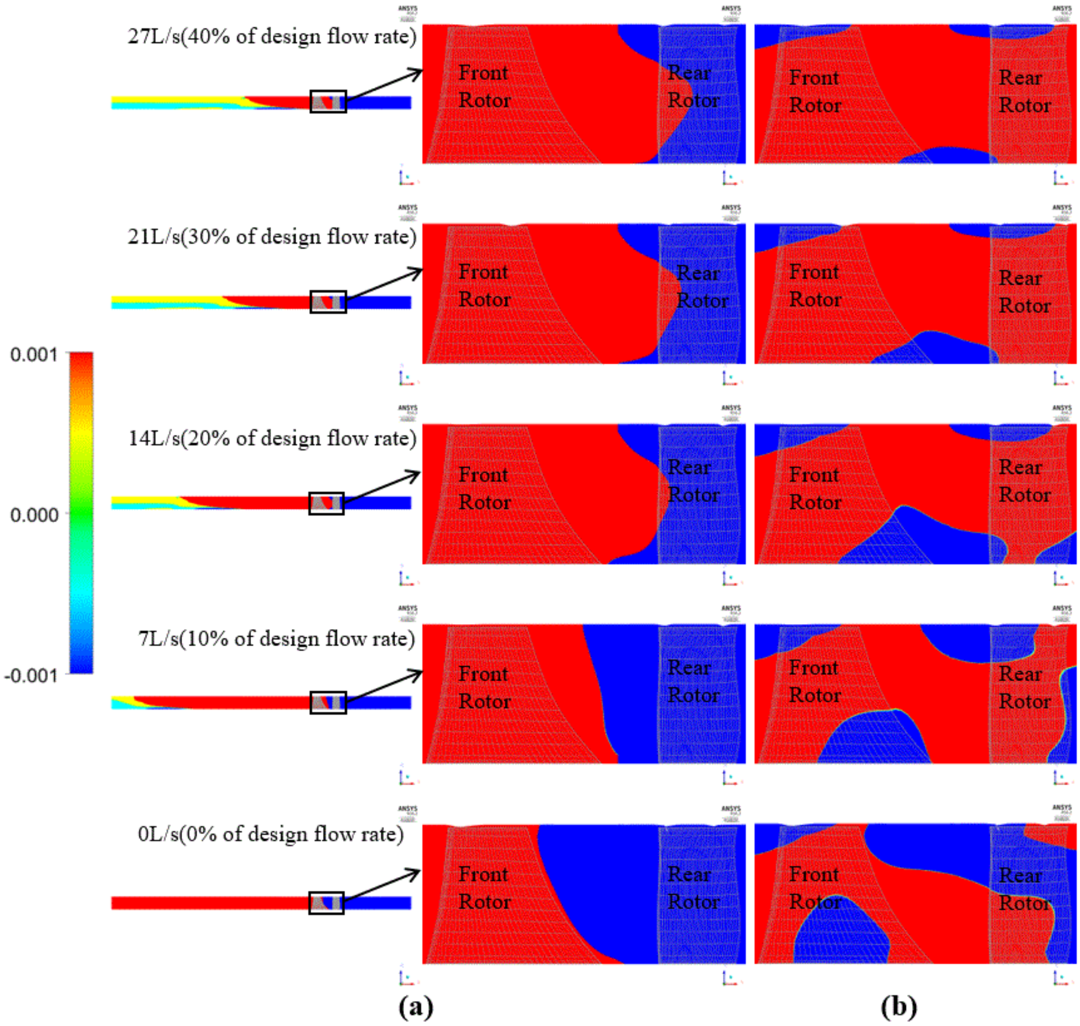

Figure 4. Contours of averaged normalized circumferential (a) and axial (b) velocities

3.1.1. Comparison of axial positions of backflow boundary and vortex cores. In order to better understand the development of backflow region, especially the backflow region of rear rotor, axial velocity is also normalized by the front rotor tip velocity. Small range (-0.001~0.001) is defined to emphasize the regions with flow moving in opposite directions (swirling in front and rear rotors rotating directions, moving in upstream and downstream directions). As shown in figure 4, red-color regions can be seen as regions with positive normalized velocities, while blue-color regions can represent regions with negative normalized velocities. Both normalized circumferential and axial velocities are not only arithmetically averaged in one relative revolution's duration but also circumferentially averaged. Figure 4 (a) displays the averaged normalized circumferential velocity distributions on the *r-z* plane in whole domains. The backflow region of front rotor grows with the reduction of flow rate, which is similar to the situation of an inducer [1]. However, the backflow region of rear rotor seems to have no significant change until the flow rate is reduced to 7 L/s (10% of the design flow rate). As shown in figure 4 (b) displaying the axial velocity distribution, a reverse flow region exists at the front rotor hub area, and with the reduction of flow rate, the reverse flow region moves upstream. We also notice that the size of the hub reverse flow grows rapidly at the flow rates from 40% to 20% of design flow rate, while the size of the hub reverse flow has no obvious change with the further decrease of flow rate. This reverse flow region grows rapidly from the flow rate of 27 L/s to 14 L/s, which seems to restrain the growth of the backflow region of rear rotor. When the flow rate is decreased to 7 L/s, this hub reverse flow region may grow to its limitation, and as the hub reverse flow region moves upstream, the suppression of hub reverse flow is weakened, then the rear rotor backflow region develops significantly to fill the space with the further reduction of flow rate.

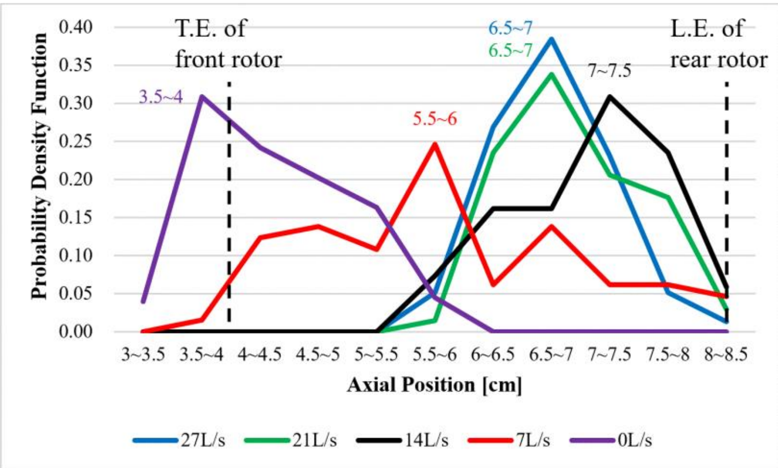

Figure 5. Axial position of backflow vortex cores on casing

Table 1. Averaged backflow region boundary axial position

Flow rates [L/s]	Boudary axial position z [cm]
27	7.264
21	7.257
14	7.336
7	5.887
0	4.366

In order to specify the axial location of vortices, we investigate the vortex cores from the limiting streamlines on casing walls for over 1000 steps (720 steps for one relative revolution of rotors), the vortex cores are checked in every 100-step, then over 60 samples are obtained at each flow rate.

Figure 5 displays the axial position of backflow vortex cores. The *y*-axis represents the probability density function of the location of vortex cores. We can find that the peak of axial location of backflow vortex cores stay near the leading edge of the rear rotor at the flow rates over 14 L/s. They stay at the nearest position to the rear rotor leading edge at 14 L/s. With the flow rate decreased from 7 L/s to 0 L/s, the axial position of vortex cores greatly moves toward the exit of front rotor.

We also compare the axial position of vortex cores with the location of rear rotor backflow boundary near the casing. In order to determine the location of the backflow region boundary, we define it by the region with small arithmetically-averaged normalized circumferential velocity between -0.001 and 0.001. Table 1 shows the results at each flow rate. We can see that this averaged backflow region boundary axial position agrees well with the axial position of vortex cores.

3.1.2. Comparison of velocities. Yokota et al [1] has found that the backflow vortex moving velocity is about the average of the maximum circumferential velocity in the main flow and the backflow. Therefore, in our simulations, the actual moving velocity of vortices, which call here "vortex observed velocity", is obtained by directly observing the vortex cores in every 100-step for total 1000 steps. At the same time, the averaged maximum circumferential velocity just upstream and downstream of vortex core is calculated, which is herein called "vortex calculated velocity". In order to make circumferential velocity available to be measured, both of observed and calculated velocities are taken at cylindrical surface with 0.975 span.

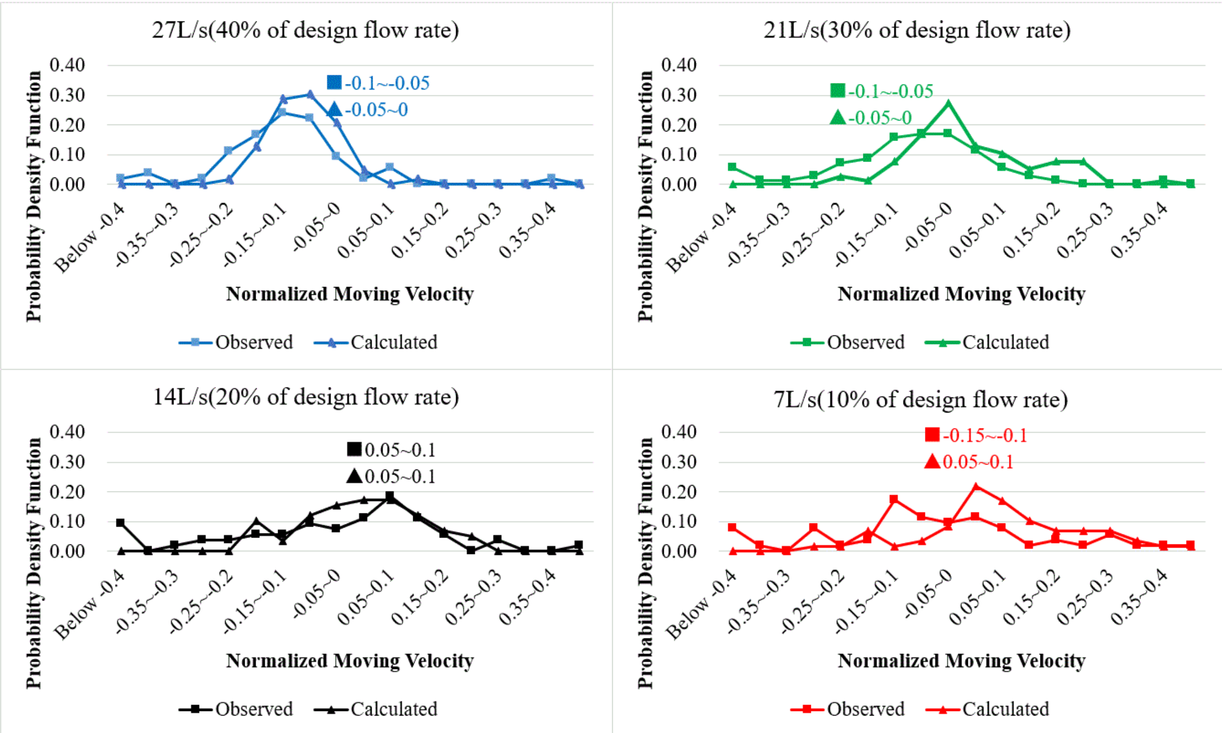

Figure 6. Comparison of the velocity observed and calculated with circumferential velocities of main flow and backflow

Figure 6 displays the comparison of probability density function of observed and calculated velocities at the flow rates below 40% of design flow rate. The vortex moving velocity has been normalized by front rotor tip velocity, therefore, the positive value denotes the vortex moving in the front rotor rotating direction, while the negative value represents the vortex moving in rear rotor rotating direction. As shown in the figure, the calculated velocity agrees well with the observed velocity from 40% to 20% of design flow rate, while at 10% of design flow rate, the peak of observed velocity distribution seems to have the opposite moving direction shown by calculated velocity distribution. At 10% of design flow rate, the vortex moving velocity shows multi-peaks distribution in observed moving velocity. As will be shown later, these observed moving velocities of vortices are related to the unsteady and aperiodic behaviour of vortices.

Based on the comparison of axial position of vortex cores and backflow region boundary as well as on the comparison of observed and calculated velocities, we believe these vortices occurring between front and rear rotors are the result of shear layer instability between main flow from front rotor and backflow of rear rotor.

3.2. Behaviours of backflow vortex
In order to be similar with the condition in experiment, these backflow vortices are also investigated on the casing wall. Two main types of backflow vortex behaviours are observed: these backflow vortices move circumferentially at the flow rates below 40% of design flow rate except 0 L/s, while the backflow vortices at 0 L/s fluctuate in high frequency around the fixed position.

3.2.1. Circumferential propagation of backflow vortex. The backflow vortices are found to circumferentially propagate on the casing at the flow rates from 40% to 10% of design flow rate. Figure 7 displays their moving velocity distributions. The central moving velocity can be found in 27 L/s, 21 L/s and 14 L/s, which indicates the stable circumferential movement of backflow vortex. We can find that there is an obvious moving direction change of central moving velocity with the decrease of flow rate. All of the central moving velocity is below 10% of front rotor tip velocity. On the other hand, the multi-peaks occur when flow rate is reduced to 7 L/s, which implies the aperiodic backflow vortex behaviour.

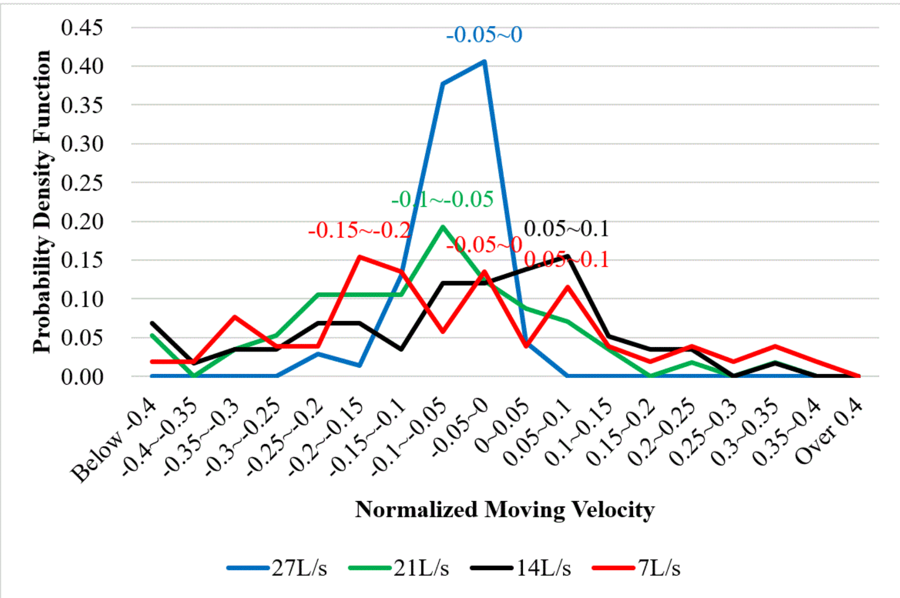

Figure 7. Normalized moving velocity distribution of backflow vortices on casing

Yokota et al [1] have found that the number of backflow vortices in an inducer is decreased with the reduction of flow rate, there is no obvious change of the number of backflow vortices in our simulation, about 5~9 at each flow rate. In our case, shearing velocity, that is defined by the circumferential velocity difference across the backflow boundary, is not significantly changed with the reduction of flow rate, which may be the reason for almost constant number of vortex forming. Otherwise, this may be caused by the limitation of RANS based simulation in unsteady flow prediction.

3.2.2. Vortex vibration in high frequency. Figure 8 shows the typical example of trajectory of vortex core on the casing at the flow rate of 0 L/s. The yellow crosses display the positions where vortex core changes its moving direction. The vortex shown in figure 8 moves from R1 to F1, then R2, F2, R3, F3, R4, F4… This moving trajectory seems like the backflow vortex vibrating at certain fixed position. Table 2 shows the trajectory information of the vortices we observed at 0 L/s, and we find these vortices take 280 ~360 steps' time in one cycle, which results in high frequency fluctuation with 81Hz~104Hz.

IOP Conf. Series: Earth and Environmental Science **163** (2018) 012036 doi:10.1088/1755-1315/163/1/012036

3.3. Experimental results

Some low frequency components occur in pressure measured in experiments at low flow rates. Figure 9 displays the FFT processed results of pressure measured at Ch.1-Ch.3 on the casing shown in figure 2.

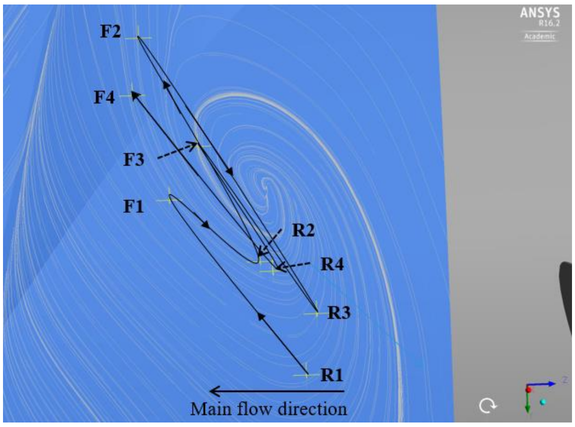

Figure 8. Trajectory of one vortex at flow rate 0L/s

Table 2. Detailed trajectory information

Vortex No.1	1	2	3	4	Average steps one cycle
R	8240	8560	8800		280
F	8320	8680	9000		340
Vortex No.2	1	2	3	4	
R	8120	8480	8800	9120	333
F	8320	8640	8920		300
Vortex No.3	1	2	3	4	
R	8320	8680	9000		340
F	8160	8440	9760	9120	320
Vortex No.4	1	2	3	4	
R	8240	8520	8880		320
F	8120	8360	8680	9000	293
Vortex No.5	1	2	3	4	
R	8160	8440	8840	9120	320
F	8280	8560	9000		360
Vortex No.6	1	2	3	4	
R	8080	8360	8720	9040	320
F	8200	8440	8920	9100	300

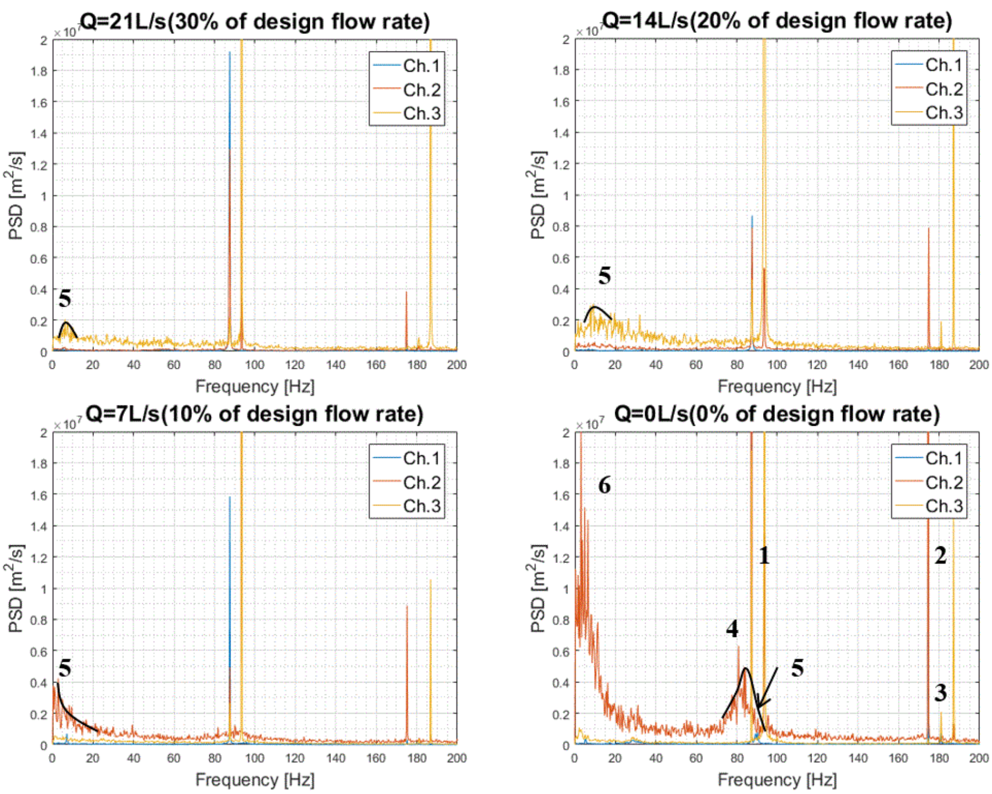

Figure 9. Pressure measured in frequency domain

Table 3. Frequency components

1	87.4Hz, 93.6Hz	BPF of front and rear rotors
2	174.8Hz, 187.2Hz	2nd harmonics of BPF of front and rear rotors
3	181Hz	Interaction of front and rear rotors
4	81.2Hz	Interaction of 2nd harmonics of rear rotor and BPF of front rotor
5	Black curves	Backflow vortex behaviour
6		Interaction of BPF of front rotor and backflow vortex behaviour

The noticeable frequency components are summarized in table 3. In the previous numerical results, backflow vortices move circumferentially in the velocity below 10% of front rotor tip velocity at flow rates 21 L/s and 14 L/s. By considering the number of vortices we observed in simulation: 5~9, their central frequency which can be calculated by (number of vortices) *(central moving velocity)/(circumference of casing) is to be below 20 Hz. In figure 9, the central frequencies smaller than 10 Hz can be seen only for Ch.3 at flow rates of 21 L/s and 14 L/s. This seems to be caused by the vortices sweeping near Ch.3. The central frequency at 14 L/s (10 Hz) is higher than that (6 Hz) at 21 L/s, which seems to be the result of distance between pressure tap Ch. 3 and backflow vortex cores position. In our simulation, compared with the axial position of vortex cores on casing at flow rate 21 L/s, vortex cores at 14 L/s exist closer to rear rotor. We also notice that the magnitude of Ch.3 at flow rate 14 L/s is larger than that at 21 L/s, which also indicates the vortex at 14 L/s is closer to Ch.3.

With the flow rate decreased to 7 L/s, pressure fluctuation is becoming more pronounced in the signal of Ch.2. In the numerical results, the backflow region of rear rotor grows rapidly when the flow rate is reduced to 7 L/s, and the backflow vortices also move upstream approaching to the location of Ch.2. Moreover, as the multi-peaks moving velocity distribution shows, these vortices slowly move with aperiodic behaviour, resulting in the low frequency pressure fluctuations near 0 Hz and weak but high frequency broad-banded fluctuations around 90 Hz.

In our simulation of flow rate 0 L/s, the backflow vortices fluctuate in a very high frequency at fixed positions as has been shown in figure 8. These vortices exist near the front rotor blade passage, indicating that these backflow vortices interact with the front rotor blades. As shown in figure 9, high frequency component occurs at flow rate 0 L/s, which should be the result of backflow vortex behaviours. As backflow vortices are too close to the front rotor blades, the nonlinear interaction between front rotor and these backflow vortices should result in the low frequency components at 0L/s.

4. Conclusions

In this study, in order to find out the causes of low frequency fluctuations observed at low flow rates in a contra-rotating axial flow pump, unsteady numerical simulations for whole front and rear rotors have been carried out. Vortex structures have been analysed especially in the region between front and rear rotors. Main findings are summarized as follows:

- Vortical structures observed between front and rear rotors seem to be the result of shear layer instability of rear rotor backflow.
- Backflow vortices between front and rear rotors locate at the boundary between main flow from front rotor and the backflow of rear rotor. They circumferentially move in a central velocity below 10% of front rotor tip velocity. This velocity roughly agrees with the averaged circumferential velocity across the backflow boundary.
- Aperiodic behaviours of backflow vortex have been observed below 10% of design flow rate, and backflow vortices at 0 L/s seem to fluctuate in a very high frequency around fixed positions.
- The low frequency components of pressure fluctuation measured in experiments seem to be the result of the slow circumferential movements of multiple backflow vortices. However, at

the flow rate of 0 L/s fluctuating motions of vortices with high frequency seem to produce the pressure fluctuation in high frequency and the interaction of front rotor and backflow vortices causes the low frequency components.

References

[1] Yokota K, Kurahara K, Kataoka D and Tsujimoto Y 1999 A study of swirling backflow and vortex structure at the inlet of an inducer *JSME International Journal* B **42** 3 pp451-459.
[2] Yamanishi N, Fukao S, Qiao X, Kato C and Tsujimoto Y 2007 LES simulation of backflow vortex structure at the inlet of an inducer *ASME Journal of Fluids Engineering* **129** pp587-594.
[3] Cao L, Honda H, Yoshimura H, Watanabe S and Furukawa A 2014 Experimental investigation of blade rows interactions in contra-rotating axial flow pump *Proc. ASME 2014 4th Joint US-European Fluids Engineering Division Summer Meeting* FEDSM2014-21901.
[4] Cao L, Watanabe S, Momosaki S, Imanishi T and Furukawa A 2013 Low speed design of rear rotor in contra-rotating axial flow pump *International Journal of Fluid Machinery and Systems* **6** 2 pp105-112.